

Contact fatigue of silicon

Sanjit Bhowmick

*Materials Science and Engineering Laboratory, National Institute of Standards and Technology,
Gaithersburg, Maryland 20899-8520*

Juan José Meléndez-Martínez

Departamento de Física, Universidad de Extremadura, 06071 Badajoz, Spain

Brian R. Lawn^{a)}

*Materials Science and Engineering Laboratory, National Institute of Standards and Technology,
Gaithersburg, Maryland 20899-8520*

(Received 20 November 2007; accepted 22 January 2008)

Macroscopic cracks in bulk silicon are generally considered to be immune to fatigue. Here, evidence for pronounced fracture-related fatigue damage in cyclic contact loading of (001) monocrystalline silicon with hard spheres of millimeter-scale radius is presented. The periodic indentation field generates ring cracks around the contact, which proliferate with continued cycling. Copious debris in the form of slabs and particulates is ejected from within the crack walls onto the specimen surface. Continued ejection leads ultimately to large-scale surface removal. The fatigue damage progressively degrades the material strength, more rapidly at higher contact load. Implications concerning the function of silicon devices, including microelectro-mechanical systems, will be briefly discussed.

I. INTRODUCTION

Silicon remains the material of choice in the semiconductor industry, largely because of its unique electronic properties. Less well studied are its mechanical properties, despite the important role of such properties in the assessment of device reliability. Silicon is highly brittle. Surface flaws and defects are easily generated by the slightest microcontacts, making this material susceptible to severe strength degradation during function.¹⁻⁹ Conventional fracture tests on specimens of silicon monocrystals containing tensile-loaded plane cracks have established that silicon has a toughness $<1 \text{ MPa m}^{1/2}$,⁹⁻¹¹ i.e., not much higher than that of glass. Other plane-crack tests on silicon have indicated no sensitivity to slow crack growth from interactions with moisture in the environment.^{9,12} Flexure tests on silicon specimens containing indentation cracks reveal no sign of any crack extension in air at stress levels incrementally below that required to cause fast fracture, over extended loading periods.¹³ This insensitivity to water is quite unique among brittle materials and is attributable to the covalent nature of the silicon bonding.¹⁴ In short, there appears to be no evidence in the literature indicating any significant fatigue effects in bulk silicon, which has prompted the conventional wisdom that materials with

diamond structure should be immune from cyclic fatigue. The plane-crack fatigue studies on silicon appear to confirm this expectation.¹⁵ In applications where periodic mechanical, electrical, or thermal stresses operate, e.g., sensor technology, electronic packaging, solar panels, and optical systems, any such absence of fatigue effects would clearly be conducive to high reliability.⁹

However, a surge of recent experiments on micromachined polysilicon specimens reports clear evidence of strength degradation in cyclic loading. High frequency cyclic loading is a characteristic feature of microelectro-mechanical system (MEMS) devices, and failures occur during function; strength losses exceeding 50% of the static loading level are typical. Different groups have reached conflicting conclusions concerning the cause. One group argues that the source is purely mechanical, perhaps arising from some kind of crack wedging, and is sensitive to the ratio of tension/compression in the load cycle.¹⁶⁻²⁰ Another group argues that the fatigue is due to the repeated buildup and rupture of a thin oxide film near the crack tip.²¹⁻²⁵ Both schools contend that any such fatigue process is likely to be limited to small-scale structures, explaining the absence of reported effects in bulk specimens. However, it is not easy to conduct definitive observations of processes within submicroscopic cracks in small-scale specimens, so the issue of fatigue in silicon remains highly controversial.

In the present study, we propose examining this issue by conducting indentation experiments on monocrystalline silicon using millimeter-scale spheres. Tests of this

^{a)}Address all correspondence to this author.
e-mail: brian.lawn@nist.gov
DOI: 10.1557/JMR.2008.0149

kind have long been used to demonstrate cone or ring cracking in silicon and other diamond structure materials.²⁶ The advantage of the spherical indenter is that it is easier to follow the evolution of fracture and deformation within a well-defined contact zone. Moreover, the stresses are intense over a localized area, and are capable of driving processes that can lead to rapid degradation of the material. Such processes might go unnoticed in more conventional tensile specimens. Sphere contact has been used to quantify cyclic fatigue in a wide range of polycrystalline and glassy ceramic materials, thus far all with at least some ionic component in the bonding and accordingly with some susceptibility to moisture-assisted slow crack growth.²⁷ The question is posed as to whether similar contact fatigue extends to relatively inert materials like silicon. A preliminary report indicates that it does, although the mechanisms appear to be quite different to those hitherto reported.²⁸ We shall examine the nature of such fatigue and demonstrate that the effects are in fact pronounced.

II. EXPERIMENTAL

Silicon {100} plates 1 mm thick and 100 mm in diameter were obtained in a highly polished state with <5 nm roughness (University Wafer, South Boston, MA). The plates were diamond scribed and carefully broken into plates 25 mm square. The resulting specimen squares were cleaned in ethanol and examined prior to testing to ensure the absence of spurious scratches and damage from the preparation.

A schematic illustration of the test procedure is shown in Fig. 1. Figure 1(a) describes the indentation process used to produce the damage pattern. The silicon surfaces were loaded with tungsten carbide (WC) spheres of radius $r = 1.6$ mm in a servo-hydraulic testing machine (model 8502, Instron Corp, Canton, MA) for a specified n cycles at a frequency of 10 Hz. Inspection in a field emission scanning electron microscope (Hitachi FE-SEM S4700) (Hitachi High Technologies, Tokyo, Japan) showed the spheres to have an asperity roughness <1 μm . The load form was haversinusoidal, with maximum loads P_m up to 550 N and a minimum load of 2 N (the latter to prevent the indenter from wandering across the surface), and maximum number of cycles in excess of $n = 10^6$. Most tests were conducted in air, but some were conducted in a water bath. Comparative tests in static loading were also performed, with rapid loading to P_m and unloading to zero and with intervening hold times spanning the range of durations in the cyclic tests, i.e., in excess of 10^7 s. Only one indentation was made on each specimen square, to avoid damage overlap.

After unloading, each indented surface was examined for the presence of contact damage in an optical microscope with Nomarski illumination. Care was taken to

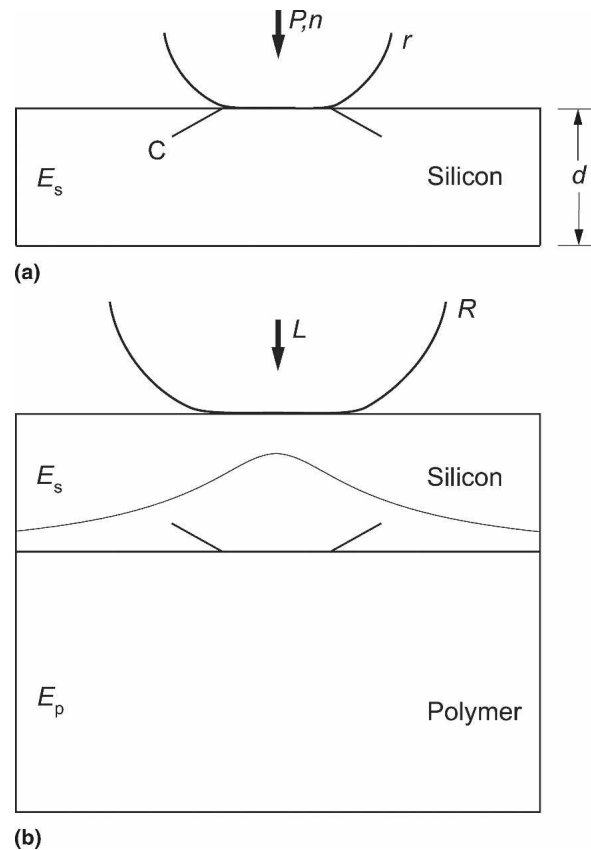


FIG. 1. Schematic diagram of the test procedure: (a) indentation on silicon plate of thickness d with WC indenter of radius r for number of cycles n at peak load P_m , producing ring crack C, (b) bilayer strength test for inverted silicon plate bonded to polycarbonate base and loaded with indenter of radius R ($\gg r$) at monotonically increasing load L . Tensile stress at bottom of plate has the form of a bell curve.

avoid any handling of the indentation sites in these examination procedures, to avoid disturbing any residual damage. The extent of damage was quantified using a commercial image analysis software package (IP Lab, Scanalytics, Fairfax, VA). The algorithm sets a threshold to exclude background information, and counts the pixels within the damaged surface area above this threshold. The equivalent integrated area is expressed as a fraction of the computed contact area. Indented surfaces were also examined by scanning electron microscopy, again with care to leave any residual damage from the indented surfaces intact. Some indentation sites were sectioned by cutting with a diamond saw and then polishing down to the contact axis.

Figure 1(b) shows a simple bilayer test configuration used to measure strengths of the indented plates.²⁹ The plates were inverted and then bonded to the indentation surface face down with a thin layer of epoxy (~ 10 μm) to a polycarbonate base 12.5 mm thick. The resulting bilayers were then centrally loaded at their top surfaces with a larger sphere, radius $R = 3.2$ mm, in a screw-driven mechanical testing machine (Instron 8500; Instron

Corp., Boston, MA). This specimen configuration places the plate undersurfaces in a state of flexure on the compliant support base and was chosen to avoid premature failures from edge flaws in the silicon. A video camera was placed below the specimen to observe the silicon bottom surface during testing. "Failure" was deemed to have occurred when a large-scale crack propagated unstably from the pre-indentation site. Critical loads (L) for this instability condition were recorded, and equivalent strengths (S) were calculated using the bilayer relation $S = (L/Bd^2)\log(E_s/E_p)$, where d is the plate thickness, $E_s/E_p = 170 \text{ GPa}/2.35 \text{ GPa} = 72.3$ is the silicon/polycarbonate modulus ratio, and $B = 2$.³⁰

III. RESULTS

A. Damage morphology

Some precursor tests were carried out to establish the critical load below which no visible cracking occurs on as-polished silicon surfaces in single-cycle loading with WC spheres $r = 1.6 \text{ mm}$ in air. This was done by placing arrays of 50 indentations in load increments up to $P = 600 \text{ N}$ on 100-mm-diameter plates and looking for the onset of ring cracks. The critical load was determined as $550 \pm 25 \text{ N}$. An additional 20 tests at $P = 500 \text{ N}$ revealed no indication of any cracks. Figure 2 shows optical micrographs of a typical ring crack pattern formed at 550 N, (001) surface view [Fig. 2(a)] and (110) section view [Fig. 2(b)]. The straight sides of the crack in the surface view reflect the fourfold symmetry of the (100) surface and correspond to traces of $\{111\}$ easy cleavage planes in the silicon structure.^{26,31,32} The downward crack traces in the section view are inclined at $30^\circ \pm 5^\circ$ relative to the surface, which lies between the 22° for classical Hertzian trajectories in glass and 55° for traces of $\{111\}$ planes on the section surface, indicating a compromise between tendencies to follow principal stress trajectories and cleavage planes.²⁶ No sign of any plastic deformation was detected optically or in the SEM at this or any other indentation site, i.e., dislocation slip lines or twins, confirming an essentially elastic–brittle response.

Figure 3 is a sequence of optical micrographs of cyclic damage patterns taken for a peak contact load $P_m = 250 \text{ N}$, i.e., less than half the critical load for ring crack initiation in a single-cycle test, in air. Each micrograph is a different specimen, so the pattern geometries show some variation. Nevertheless, the evolution of damage is apparent. The white circles artificially superimposed onto the micrographs indicate the contact radius evaluated from Hertzian elastic contact theory.^{27,33} A faint imprint of the indenter is observed within this circle. Surface profilometry of such imprints prior to any cracking showed no measurable surface depression, typical of superficial "fretting" damage from asperity microcontacts. No fracture is observed until after about $n = 10^3$

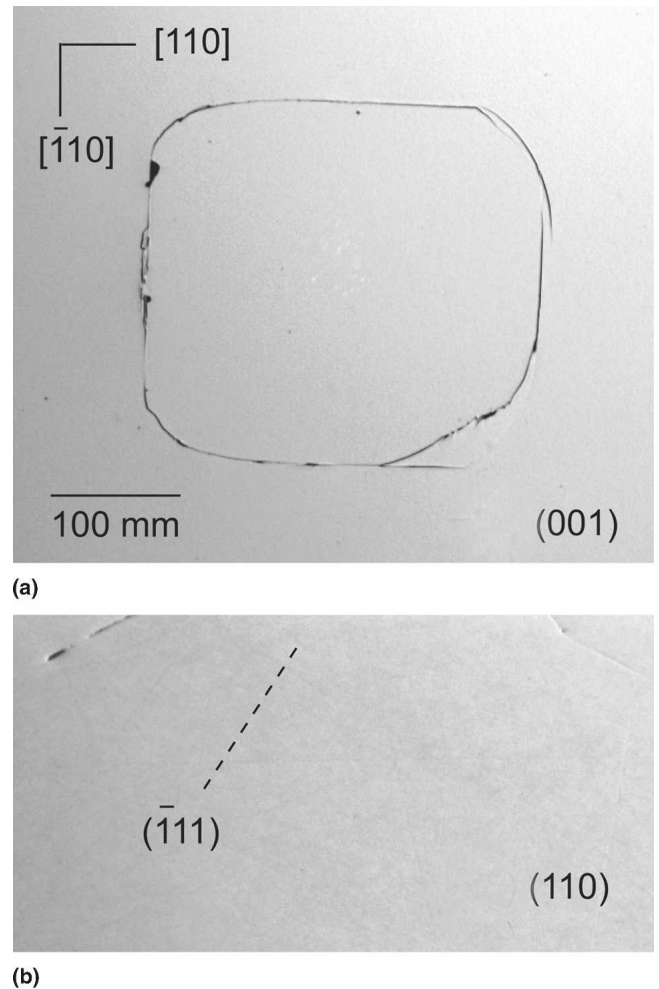


FIG. 2. Optical micrographs of ring crack in silicon from single-cycle loading of WC indenter, radius $r = 1.6 \text{ mm}$ at load 550 N, showing crack geometry on (a) (001) top surface and (b) (110) section surface. Dashed line in (b) indicates trace of preferred cleavage plane. Note crystallographic influence on crack traces.

cycles, at which point a full ring crack forms [Fig. 3(a)]. Two of the ring crack edges intersect the contact circle, suggesting that the crack has initiated from a contact-induced flaw. The asymmetry of the ring crack pattern, with those ring segments opposite the initiation points well outside the contact circle, is attributable to "pseudo inertia" as the crack circumvents the contact.³⁴ On continuing the cycling to $n = 5 \times 10^3$, some form of surface debris begins to appear at some of the crack segments [Fig. 3(b)]. At $n = 20 \times 10^3$, the damage becomes more intense, and multiple cracking appears [Fig. 3(c)]. At $n = 85 \times 10^3$, some chips have formed around the contact, leading to detachment of collars of material [Fig. 3(d)]. Finally, at $n = 200 \times 10^3$, the indenter has penetrated the surface, with copious ejection of material, leaving a "black hole" [Fig. 3(e)].

The nature of the cyclic fatigue damage is more clearly discerned from scanning electron micrographs in Figs. 4

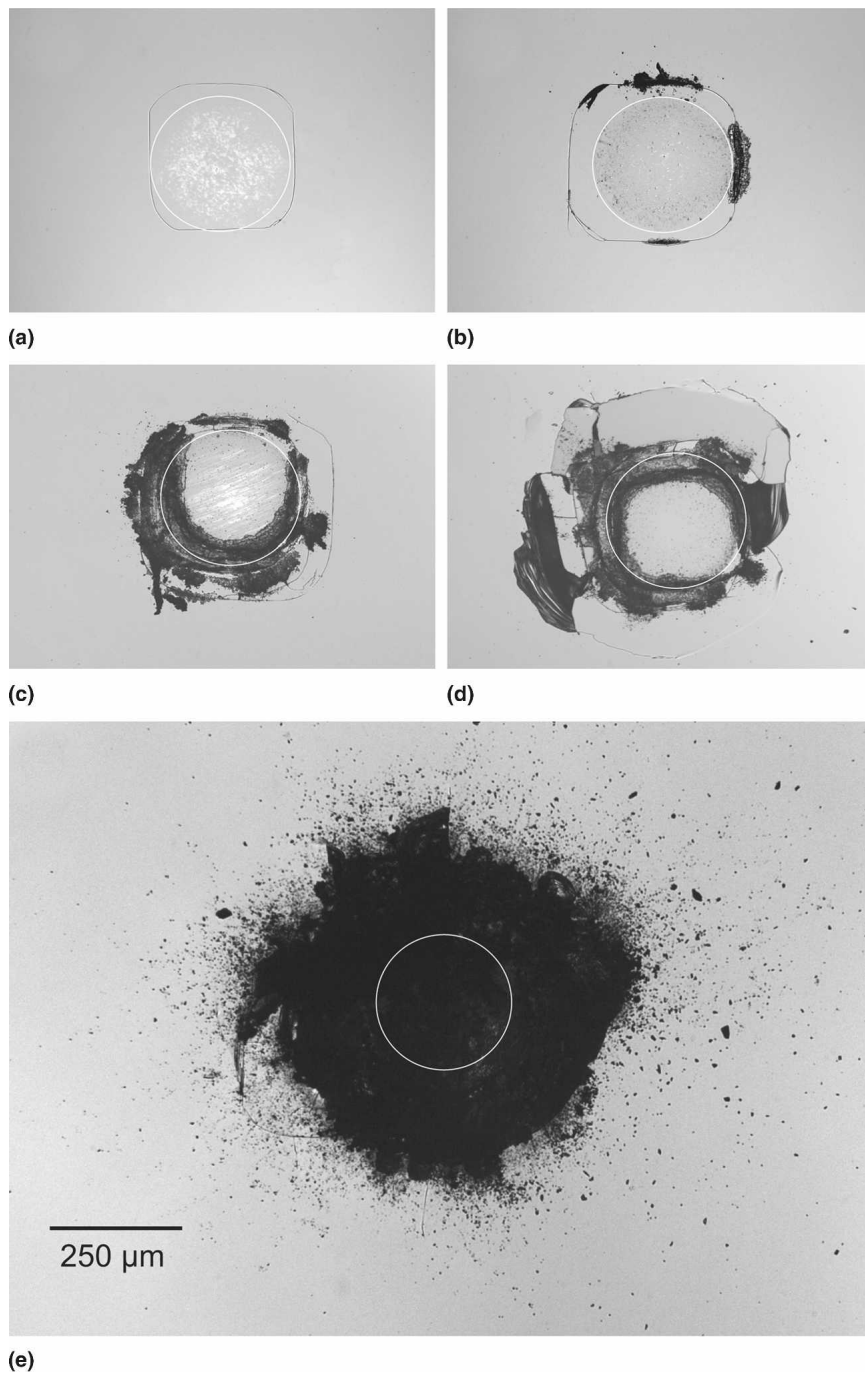
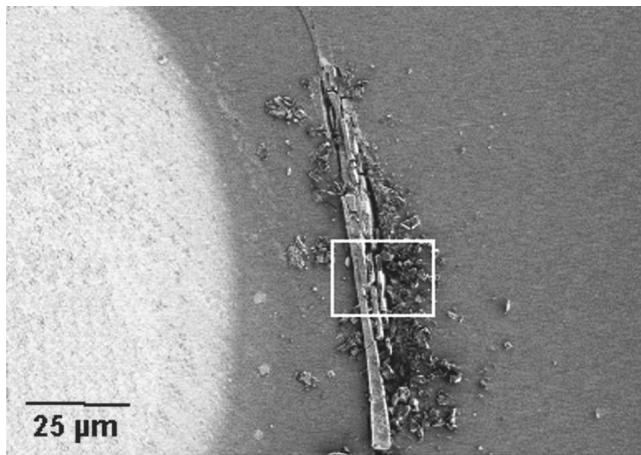


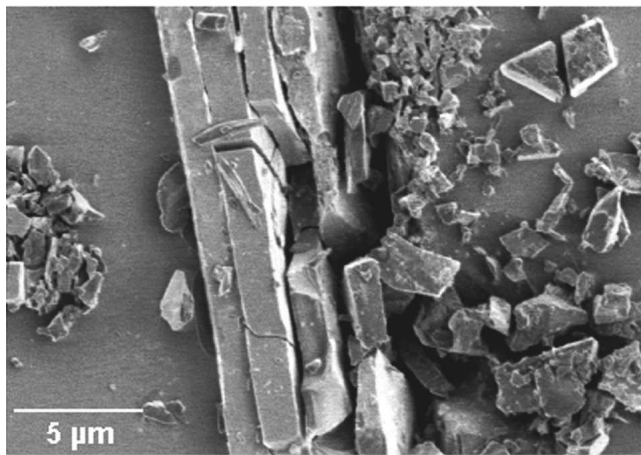
FIG. 3. Optical micrographs of contact damage in (001) silicon, from cyclic loading of WC indenter, $r = 1.6$ mm, at $P_m = 250$ N: (a) $n = 1 \times 10^3$, (b) $n = 5 \times 10^3$, (c) $n = 20 \times 10^3$, (d) $n = 85 \times 10^3$, and (e) $n = 200 \times 10^3$ cycles. Each micrograph is a separate specimen. White circle designates contact area computed from Hertzian elasticity theory.

and 5, again for tests in air at $P_m = 250$ N. Figure 4(a) shows a ring crack segment well outside the contact area (the latter apparent as the white region at left) at $n = 5 \times 10^3$ cycles, where tensile stresses operate. A view of the region within the rectangular inset in this figure is reproduced at higher magnification in Fig. 4(b). Substantial quantities of slab and particulate ejecta are observed around the crack trace. These ejecta appear to have some

kind of crystallographic morphology. Figure 5 shows crack segments closer to the contact circle (superimposed white lines), after (a) $n = 5 \times 10^3$ cycles and (b) $n = 20 \times 10^3$ cycles. In the first case, the damage consists of several parallel crack segments 1–5 μm apart, with minor particulate production [Fig. 5(a)]. In the second case, the multiplicity of cracking remains, but the additional cycling has produced copious debris, heavily



(a)



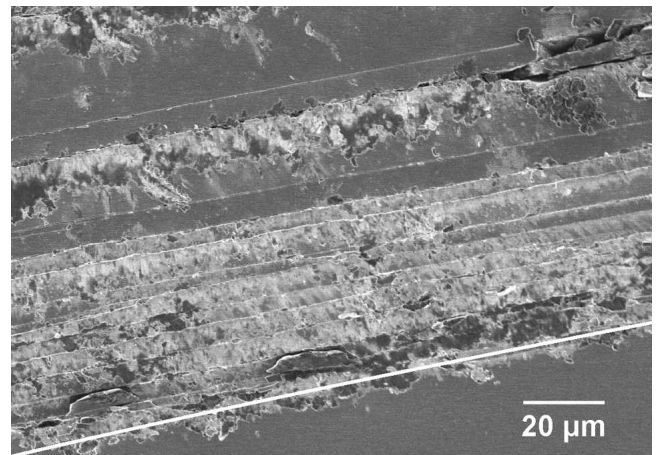
(b)

FIG. 4. FE-SEM images of (a) ring crack segment in (001) silicon, from cyclic loading of WC indenter, $r = 1.6$ mm, at load $P_m = 250$ N for $n = 5 \times 10^3$ cycles, showing plate and particulate ejecta on surface at ring crack segment well outside contact. The photo in (b) is a high-magnification view of the inset in (a). Contact area is evident as white region at left in (a).

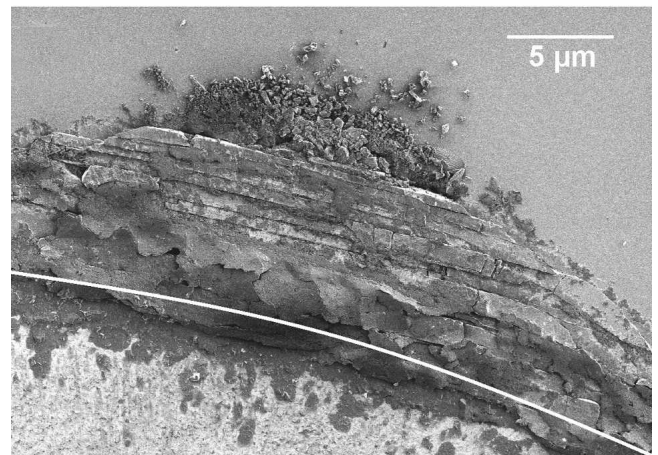
smear out close to the contact circle [Fig. 5(b)]. The scale of this damage is suggestive of some kind of internal mechanical process within the ring-crack walls, with a capacity to proliferate during cycling.

B. Damage quantification

Additional tests were conducted to determine the critical number of cycles n_1 to initiate ring cracks for any given peak applied load P_m . This was done by making arrays of indentations over a range of cycles and determining the lower bounds to n_1 , below which cracks never appeared, and upper bounds, above which cracks always appeared. These bounds, along with their (logarithmic) means, are plotted in Fig. 6 over a range of P_m . The box at $n_1 = 1$ at the left axis represents the critical load for initiation in single-cycle indentation. A rapid increase in



(a)



(b)

FIG. 5. Field emission scanning electron-microscope images of indented (001) silicon with WC indenter, $r = 1.6$ mm, at $P_m = 250$ N showing damage at crack traces immediately outside contact: (a) multiple cracking after $n = 10 \times 10^3$ cycles and (b) smeared particulate matter after $n = 20 \times 10^3$ cycles. The contact circle is indicated by white circular segments. Note smearing of ejected material in (b).

n_1 with decreasing P_m is apparent, consistent with a diminution in stress field intensity at lower loads.

Quantification of the damage intensity after ring-crack initiation is given in Fig. 7. This figure plots the fractional pixel count of surface damage area relative to elastic contact area (white circles) as a function of number of cycles, from optical micrographs like those shown in Fig. 3. In this plot, the threshold in the image analysis algorithm was set to exclude counts from the undamaged silicon surfaces plus spurious fretting damage within the contact. Results are shown for loads $P_m = 400, 250,$ and 100 N. Symbols indicate data for contacts with ring cracks: unfilled symbols, ring cracks with no attendant damage; filled symbols, cracks with measurable debris and chipping. The vertical shaded bands indicate the range of cycles over which initiation first occurred, taken from Fig. 6. The solid lines are empirical fits to the data

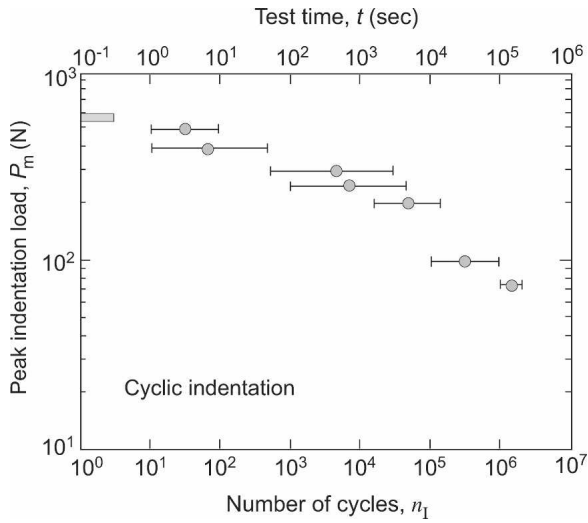


FIG. 6. Plot showing the number of cycles n_1 to initiate ring crack with WC indenter, $r = 1.6$ mm, on (001) silicon at different peak loads P_m . Bands indicate spreads in cyclic range. The box at the left axis represents critical load for initiation in single-cycle indentation.

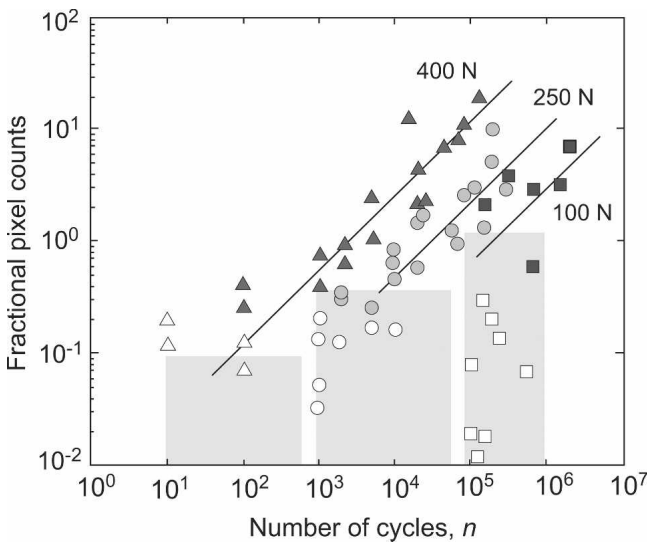


FIG. 7. Area of surface damage normalized to contact area as function of number of cycles n for indentations on (001) silicon with WC indenter, $r = 1.6$ mm, at loads $P_m = 100, 250,$ and 400 N. The solid line is the empirical linear fit; grey bands indicate threshold number of cycles for initiation of ring cracks (from Fig. 6).

with slope unity (logarithmic coordinates) for cracks with debris. These results demonstrate an approximately linear increase in damage intensity with cycling beyond some incubation stage of ring crack formation and debris production, with diminished rates at lower contact loads.

C. Strength of indented surfaces

A set of tests was run to determine strength of silicon plates after conventional single-cycle indentation, using the configuration in Fig. 1(b). Results are shown in Fig. 8 for tests on air. Data points are means and standard

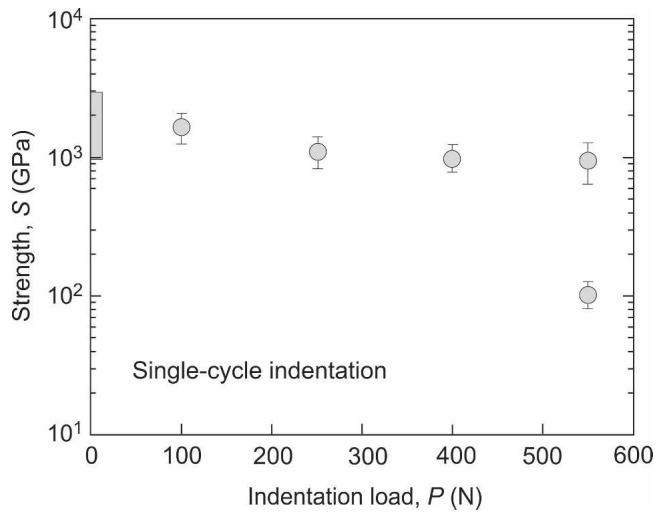


FIG. 8. Strength of (001) silicon plates after single-cycle indentation as function of load. The box at the left axis represents critical load for crack initiation in unindented surfaces. Error bars are standard deviations.

deviations for indented surfaces. The box on the left axis at $P = 0$ indicates the strength of as-polished (i.e., unindented) surfaces. There is a slight but systematic decline in strength with increasing load until, at $P = 550$ N, the data split into two levels: those data at the upper strength level correspond to indentations without ring cracks, those at the lower level to indentations with well-formed cracks. The fact that the strengths for surfaces with low-load indentations is only marginally lower than those for unindented surfaces indicates that the asperity damage responsible for the strength decrement is only slightly more severe than polishing flaws. At indentation loads at 600 N and above, the specimens fractured during loading, precluding extension of the data range.

Figure 9 shows strengths of silicon plates indented under fatigue conditions, as a function of number of cycles n (cyclic tests) or equivalent load time t (static tests), for 4 peak loads P_m . All data points in this figure represent failures from indentation sites. Filled symbols represent cyclic data, unfilled symbols static data; circles represent tests in air; triangles represent tests in water. Boxes on the left axes indicate standard deviation bounds for specimens containing single-cycle indentations, from Fig. 8. Consider first the plot for $P_m = 550$ N [Fig. 9(a)]. The data are distributed almost equally in two distinct bands: upper band, around 1 GPa, corresponding to indentations without ring cracks; and lower band, around 100 MPa, corresponding to indentations with ring cracks. Importantly, the static data at each level show no detectable decline over the time range covered, thus confirming the absence of any significant slow crack growth. The cyclic data in Fig. 9(a) are limited—again, most specimens fractured spontaneously after just a few cycles. Those few specimens that survived 10 cycles had

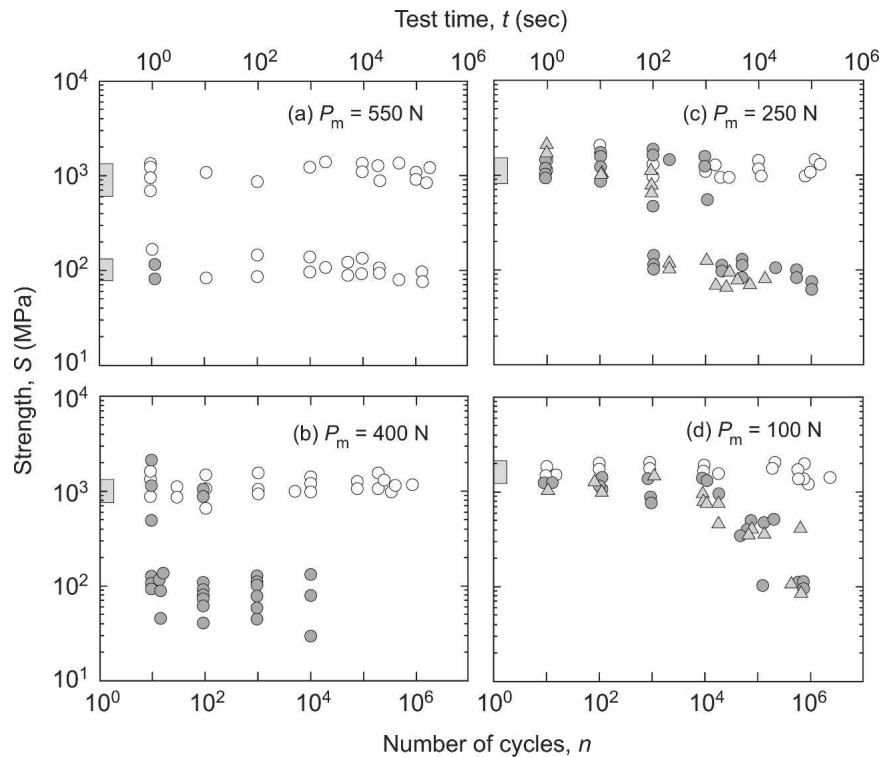


FIG. 9. Strength of (001) silicon plates after static and cyclic indentation experiments with WC sphere, $r = 1.6$ mm, at loads (a) $P_m = 550$ N, (b) 400 N, (c) 250 N, and (d) 100 N plotted as a function of the number of cycles n (cyclic tests) or equivalent peak load hold time t (static tests). Filled symbols represent cyclic data, unfilled symbols static data. Circles represent tests in air, triangles tests in water. Boxes at the left axis are means and standard deviations for single-cycle tests ($n = 1$).

strengths coincident with the lower level for static loading.

Next, consider the data for the lower loads, i.e., $P_m = 400$ N [Fig. 9(b)], $P_m = 250$ N [Fig. 9(c)], and $P_m = 100$ N [Fig. 9(d)]. At these loads, static indentation produces no ring cracks, confining the strength data to the upper band. Again, the static data at any given load show no detectable decline with indentation time. However, the upper-band strength levels do show a slight but systematic relative increase through Figs. 9(b)–9(d), consistent with the trend in Fig. 8, suggesting that the flaws induced by indenter asperities become more severe with increasing indentation load. The cyclic data show the same drop off to the lower strength band as in Fig. 9(a), but now only after an incubation number of cycles for ring-crack formation. This incubation phase becomes more protracted with diminishing indentation load until, at $P_m = 100$ N, significant falloff occurs only after about 10^5 cycles. Interestingly, the tendency to further decline in strength in the lower-band region is only slight. Taken together with the morphological evidence in Fig. 3, this indicates multiplication rather than deepening of the ring cracks responsible for the strength loss. Note that data for indentations in air and water overlap within the scatter [Figs. 9(c) and 9(d)], again consistent with the absence of any significant rate effects in the crack growth from moisture.

IV. DISCUSSION

The indentation results presented in this study demonstrate the existence of cyclic fatigue in bulk monocrystalline silicon. The fatigue is manifested as a delayed ring crack initiation followed by pronounced crack proliferation and accumulation of fracture debris at the contact sites. Flexure tests on indented specimens show substantial strength losses beyond a critical number of cycles at which ring cracks form, but relatively minor losses thereafter, indicating little continued crack deepening. Comparative cyclic tests in air and water show no detectable differences in strength loss, and static indentation tests over extended loading periods reveal no strength losses at all, confirming the absence of any moisture-enhanced slow crack growth in the fatigue process. These results, together with the tectonic appearance of the slab-like and particulate debris, are highly suggestive of a mechanical fatigue process.

Different stages in the cyclic fatigue process are apparent. In the first stage, an imprint of the contact develops, as micrometer-scale asperities on the spherical indenter induce localized microplasticity zones in the silicon surface. These zones are subject to intensification with continued cycling, manifested as surface “fretting” at the periodically expanding and contracting contact between elastically mismatched indenter and specimen.³³ Such

microplasticity zones are quite capable of generating microcracks, the dimensions of which may be expected to scale with those of the damage zones themselves, i.e., in the micrometer range.⁸ Such flaw size is consistent with the upper-level strength $S \approx 1$ GPa in Fig. 8, as can be seen by inserting toughness $T \approx 1$ MPa m^{1/2} for silicon and flaw-geometry coefficient $\psi = 1$ into the well-documented Griffith relation to obtain $c_f = (T/\psi S)^2 \approx 1$ μm .⁷ The issue as to how the offending microcracks increase in severity with progressive cycling is yet to be elucidated.³

This first stage in the fatigue may be considered somewhat superficial, since it involves nothing more than a surface-localized wear process. Nevertheless, it produces flaws in the same range of strength (1 GPa or higher) or size (1 μm or lower) as measured in experiments on micromachined specimens.^{17,21,35,36} It is of interest to observe how the current data compare with published fatigue data on small-scale specimens, usually expressed as peak cyclic stress versus number of cycles to failure. Such data have been collapsed onto the universal fatigue plot shown in Fig. 10, by normalizing peak stress σ_m to the single-cycle value σ_1 for crack initiation.³⁷ We have incorporated our own data from Fig. 6 into the same plot by adopting the simple relation $\sigma_m/\sigma_1 = (P_m/P_1)^{1/3}$ between stress σ and contact load P from Hertzian elasticity theory.²⁷ The fact that all data in Fig. 10 show a similar trend—within the bounds of scatter—might be taken as indication of a common fatigue process in small-scale flaws. This is an appealing prospect but requires more detailed investigation.

The next stage in the fatigue process, that of extensive degradation of the silicon surfaces after the onset of first ring cracking, is visually more striking. As seen in Figs. 3–5, ejection of slabs and particulates from within the

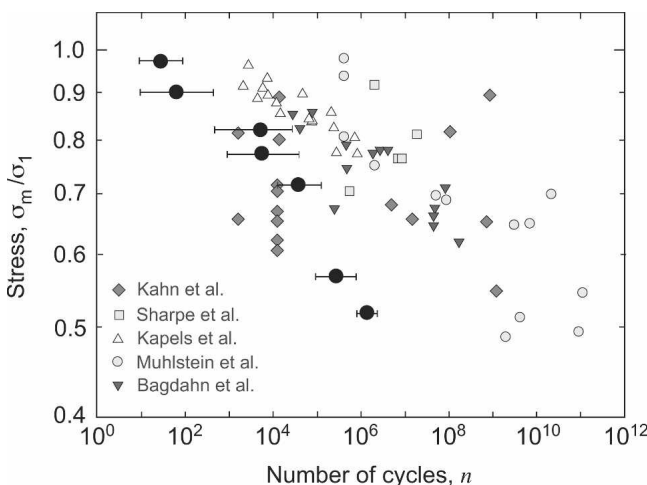


FIG. 10. Comparing current fatigue behavior of bulk silicon with literature data from micro-scale specimens. Current data are shown as large symbols with error bands (from Fig. 6). Other data are from compilation in Ref. 37.

crack walls and proliferation of ring cracking generates an ever-increasing surface damage pattern with progressive cycling. The nature of the debris suggests some kind of frictional sliding at the crack walls. Such friction is consistent with a small but not insignificant component of shear stress on the crack planes—recall the compromise between tendencies to follow principal stress trajectories and cleavage planes evident in the ring crack traces in the monocrystalline silicon. The presence of steps and surface roughness that characterize the crack walls of most brittle solids, including silicon,³⁸ could provide sources for platelet and particle detachment and eventual expulsion. With continued reverse sliding of opposing crack walls and associated production of debris, any such interfacial friction will diminish with time, thus enhancing surface displacement offsets and spreading the damage. The production of surface detritus is reminiscent of the damage accumulation that occurs in tough, coarse-grain ceramics by grain-boundary sliding under confined shear stresses,^{39–41} but there the mode is one of quasiplasticity beneath the contact whereas in the present case there is no evidence of any analogous yield mode.

A third stage in the fatigue may be identified. This refers to the smearing and crushing of ejected plates and debris at ring crack segments closer to the contact circle, evident in Fig. 5. In this context, it needs to be remembered that the gap between indenter and specimen surface remains small immediately outside the contact circle, given by $D(X) = (a^2/\pi r) [(\rho^2/a^2 - 1)^{1/2} + (\rho^2/a^2 - 2) \arctan(\rho^2/a^2 - 1)^{1/2}]$, where $X = \rho - a$ is the radial distance outside the contact with a elastic contact radius, r indenter radius, and ρ radial distance from the contact center.³³ The gap profile is shown for the current conditions of testing in Fig. 11. In the earlier stages of development, the upward displacements of the material adjoining ring crack segments remain smaller than D [Fig. 5(a)], but continued cycling increases these displacements until the material makes contact with the indenter [Fig. 5(b)]. Beyond this point, the indenter begins to compress the protruding material, spreading it into a smear layer. Ultimately, as crushed material is squeezed out from the

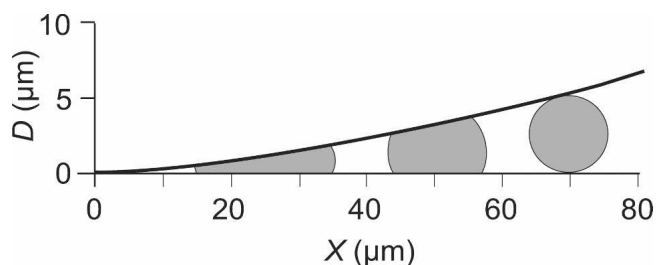


FIG. 11. Computed Hertzian contact profile, showing how 5- μm particles become trapped and smeared within the immediate gap outside elastic contact between sphere indenter and flat silicon surface.

contact zone, the indenter penetrates into the specimen surface and leaves a characteristic black hole.

The question remains as to the universality of the fatigue process observed in the current experiments. We have confined our tests to monocrystalline silicon with just one surface orientation, i.e., {100}. Will the same effect be observed with the same degree of intensity on surfaces with other crystallographic orientations, or on polysilicon? Will it extend to other diamond-structure materials, or indeed to other highly brittle materials? Will it occur with other indentation, or similarly complex, stress fields? Will the same mechanisms of fatigue be observed as the indenter radius is made smaller, approaching the micrometer scale and below? In this context, we would point out that plasticity-free ring crack formation has been observed in diamond-structure materials down to the microscale.^{42,43} What is the nature of the debris on the silicon surfaces, e.g., is it amorphous or phase-transformed? How then may the present observations bear on the fatigue failure of microelectromechanical systems and similar small-scale devices, as reported in the literature? Studies of these questions are under way.

ACKNOWLEDGMENT

Certain equipment, instruments, or materials are identified in this paper to specify experimental details; this does not imply recommendation by the National Institute of Standards and Technology.

REFERENCES

- J.G. Bradby, J.S. Williams, J. Wong-Leung, M.V. Swain, and P. Munroe: Mechanical deformation in silicon by micro-indentation. *J. Mater. Res.* **16**, 1500 (2001).
- J.G. Bradby, J.S. Williams, J. Wong-Leung, S.O. Kucheyev, M.V. Swain, and P. Munroe: Spherical indentation of compound semiconductors. *Philos. Mag. A* **82**, 1931 (2002).
- I. Zarudi, L.C. Zhang, and M.V. Swain: Microstructure evolution in monocrystalline silicon in cyclic microindentations. *J. Mater. Res.* **18**, 758 (2003).
- I. Zarudi, L.C. Zhang, and M.V. Swain: Behavior of monocrystalline silicon under cyclic microindentations with a spherical indenter. *Appl. Phys. Lett.* **82**, 1027 (2003).
- I. Zarudi, L.C. Zhang, and M.V. Swain: Effect of water on the mechanical response of monocrystalline silicon to repeated micro-indentation. *Key Eng. Mater.* **233-236**, 609 (2003).
- I. Zarudi, J. Zou, W. McBride, and L.C. Zhang: Amorphous structures induced in monocrystalline silicon by mechanical loading. *Appl. Phys. Lett.* **85**, 932 (2004).
- B.R. Lawn: Fracture and deformation in brittle solids: A perspective on the issue of scale. *J. Mater. Res.* **19**, 22 (2004).
- Y-G. Jung, A. Pajares, R. Banerjee, and B.R. Lawn: Strength of silicon, sapphire and glass in the subthreshold flaw region. *Acta Mater.* **52**, 3459 (2004).
- R.F. Cook: Strength and sharp contact fracture of silicon. *J. Mater. Sci.* **41**, 841 (2006).
- R.J. Jaccodine: Surface energy of germanium and silicon. *J. Electrochem. Soc.* **109**, C203 (1962).
- C.P. Chen and M.H. Leopold: Fracture toughness of silicon. *Am. Ceram. Soc. Bull.* **59**, 469 (1980).
- T.J. Chen and W.J. Knapp: The fracture of single-crystal silicon under various environments. *J. Am. Ceram. Soc.* **63**, 225 (1980).
- B.R. Lawn, D.B. Marshall, and P. Chantikul: Mechanics of strength degrading flaws in silicon. *J. Mater. Sci.* **16**, 1769 (1981).
- T.A. Michalske and S.W. Freiman: A molecular interpretation of stress corrosion in silica. *Nature* **295**, 511 (1981).
- E.D. Renuart, A.M. Fitzgerald, T.W. Kenny, and R.H. Dauskardt: Fatigue crack growth in micromachined single-crystal silicon. *J. Mater. Res.* **19**, 2635 (2004).
- R. Ballarini, R.L. Mullen, Y. Yin, H. Kahn, S. Stemmer, and A.H. Heuer: The fracture toughness of polysilicon devices: A first report. *J. Mater. Res.* **12**, 915 (1997).
- H. Kahn, R. Ballarini, R.L. Mullen, and A.H. Heuer: Electrostatically actuated failure of microfabricated polysilicon fracture mechanics specimens. *Proc. R. Soc. London Ser. A* **455**, 3807 (1999).
- H. Kahn, N. Tayebi, R. Ballarini, R.L. Mullen, and A.H. Heuer: Fracture toughness of polysilicon MEMS devices. *Sens. Actuators, A* **82**, 274 (2000).
- H. Kahn, R. Ballarini, J.J. Bellante, and A.H. Heuer: Fatigue failure in polysilicon not due to simple stress corrosion cracking. *Science* **298**, 1215 (2002).
- H. Kahn, R. Ballarini, and A.H. Heuer: Dynamic fatigue of silicon. *Curr. Opin. Solid State Mater. Sci.* **8**, 71 (2004).
- C.L. Muhlstein, S.B. Brown, and R.O. Ritchie: High-cycle fatigue and durability of polycrystalline silicon thin films in air. *Sens. Actuators, A* **94**, 177 (2001).
- C.L. Muhlstein, E.A. Stach, and R.O. Ritchie: A reaction-layer mechanism for the delayed failure of micron-scale polycrystalline silicon structural films subjected to high-cycle fatigue loading. *Acta Mater.* **50**, 3579 (2002).
- P. Shrotriya, S. Allameh, S. Brown, Z. Suo, and W.O. Soboyejo: Fatigue damage evolution in silicon films for micromechanical applications. *Exp. Mech.* **43**, 289 (2003).
- D.A. Alsem, O.N. Pierron, E.A. Stach, C.L. Muhlstein, and R.O. Ritchie: Mechanisms for fatigue of micron-scale silicon structural films. *Adv. Eng. Mater.* **9**, 15 (2007).
- O.N. Pierron and C.L. Muhlstein: The role of debris-induced cantilever effects in cyclic fatigue of micron-scale silicon films. *Fatigue Fract. Eng. Mater. Struct.* **30**, 57 (2007).
- B.R. Lawn: Hertzian fracture in single crystals with the diamond structure. *J. Appl. Phys.* **39**, 4828 (1968).
- B.R. Lawn: Indentation of ceramics with spheres: A century after Hertz. *J. Am. Ceram. Soc.* **81**, 1977 (1998).
- S. Bhowmick, J.J. Meléndez-Martínez, and B.R. Lawn: Bulk silicon is susceptible to fatigue. *Appl. Phys. Lett.* **91**, 201902 (2007).
- H. Chai, B.R. Lawn, and S. Wuttiphon: Fracture modes in brittle coatings with large interlayer modulus mismatch. *J. Mater. Res.* **14**, 3805 (1999).
- P. Miranda, A. Pajares, F. Guiberteau, Y. Deng, and B.R. Lawn: Designing damage-resistant brittle-coating structures: I. Bilayers. *Acta Mater.* **51**, 4347 (2003).
- V.R. Howes and S. Tolansky: Pressure crack figures on diamond faces: I. The octahedral face. *Proc. R. Soc. London Ser. A* **230**, 287 (1955).
- V.R. Howes and S. Tolansky: Pressure crack figures on diamond faces: II. The dodecahedral and cubic faces. *Proc. R. Soc. London Ser. A* **230**, 294 (1955).
- K.L. Johnson: *Contact Mechanics* (Cambridge University Press, London, UK, 1985).
- F.C. Frank and B.R. Lawn: On the theory of hertzian fracture. *Proc. R. Soc. London Ser. A* **299**, 291 (1967).

35. H. Kapels, R. Aigner, and J. Binder: Fracture strength and fatigue of polysilicon determined by a novel thermal actuator. *IEEE Trans. Electron Dev.* **47**, 1522 (2000).
36. W.N. Sharpe, K.M. Jackson, K.J. Hemker, and Z.L. Xie: Effect of specimen size on young's modulus and fracture strength of polysilicon. *J. Microelectromech. Syst.* **10**, 317 (2001).
37. N. Bagdahn and W.N. Sharpe: Fatigue of polycrystalline silicon under long-term cyclic loading. *Sens. Actuators, A: Phys.* **103**, 9 (2003).
38. J.S. Williams, B.R. Lawn, and M.V. Swain: Cone crack closure in brittle solids. *Phys. Status Solidi A* **2**, 7 (1970).
39. S. Lathabai, J. Rödel, and B.R. Lawn: Cyclic fatigue from frictional degradation at bridging grains in alumina. *J. Am. Ceram. Soc.* **74**, 1340 (1991).
40. B.R. Lawn, N.P. Padture, H. Cai, and F. Guiberteau: Making ceramics 'ductile'. *Science* **263**, 1114 (1994).
41. N.P. Padture and B.R. Lawn: Contact fatigue of a silicon carbide with a heterogeneous grain structure. *J. Am. Ceram. Soc.* **78**, 1431 (1995).
42. S. Tolansky and V.R. Howes: Induction of ring cracks on diamond surfaces. *Proc. Phys. Soc. London Ser. B* **70**, 521 (1957).
43. B.R. Lawn: Partial cone crack formation in a brittle material loaded with a sliding indenter. *Proc. R. Soc. London Ser. A* **299**, 307 (1967).